ENGINEERING

Liquid seal for compact micropiston actuation at the capillary tip

Antoine Barbot[1]*, Maura Power[1], Florent Seichepine[1], Guang-Zhong Yang[2]*

Actuators at the tip of a submillimetric catheter could facilitate in vivo interventional procedures at cellular scales by enabling tissue biopsy and manipulation or supporting active micro-optics. However, the dominance of frictional forces at this scale makes classical mechanism problematic. Here, we report the design of a microscale piston, with a maximum dimension of 150 μm, fabricated with two-photon lithography onto the tip of 140-μm-diameter capillaries. An oil drop method is used to create a seal between the piston and the cylinder that prevents any leakage below 185-mbar pressure difference while providing lubricated friction between moving parts. This piston generates forces that increase linearly with pressure up to 130 μN without breaking the liquid seal. The practical value of the design is demonstrated with its integration with a microgripper that can grasp, move, and release 50-μm microspheres. Such a mechanism opens the way to micrometer-size catheter actuation.

INTRODUCTION

With increasing demand for targeted therapy and cell-based intervention, there is a growing interest in the development of new microtools that can be used for in situ and in vitro applications (*1*). Scaling down and assembling conventional tendon-driven surgical tools become infeasible when below a few hundred micrometers due to increasing surface friction forces. On the other hand, microscale tools with electromechanical actuators necessitate a large actuator footprint compared to the end effector and can have a relatively low output power. Alternative solutions have, therefore, been proposed to bring actuation to microscale tethered tools. Stimuli-responsive materials, such as light-actuated polymers, have been demonstrated to create grippers that can be placed at the end of optical fibers (*2*). Magnetic forces have also been used to actuate catheters and other medical tools with an external magnetic field. An electromagnet embedded at the tip of a 5-mm catheter to actuate a millimetric gripper has been demonstrated (*3*). One major drawback of the magnetic approaches is the rapid decay of the field gradient with distance, which requires electromagnets of several centimeters (*4*) placed close to the gripper or within a magnetic resonance imaging machine (*5*) to achieve sufficient force at smaller scales. Moreover, the forces generated by electromagnets and shape-memory materials scale down with the volume of the material and, thus, these forces become negligible for smaller designs compared to surface-based forces such as pressure or friction. More efficient pneumatic-based actuators compared to the previously mentioned technologies have been reported at micrometer and millimeter scales with a larger force output of two to three orders of magnitude (*6*). To provide actuation at the scale of a few hundreds of micrometers, we propose the combination of pneumatic actuation and surface tension to drive a piston that is attached to the distal end of a 140-μm-diameter glass capillary. The translational motion of the piston could serve as the basis of many different micromechanisms such as biopsy grippers (*7*), targeted delivery systems, and single-cell manipulation or for the orientation of micro-optics on microcatheter tips. A microgripper is chosen in this work to demonstrate the usability of the micropiston. One advantage of pneumatic actuation is that the achievable forces remain relatively large at microscales. Pressure forces depend on the surface and they scale down by a power of 2, whereas volumetric forces, such as magnetism, heat, or light, scale down by a power of 3. However, scaling down from mesoscale to microscale itself raises many challenges. Namely, to design a basic piston capable of generating mechanical force and consequently induce a displacement, a pressure differential needs to be maintained. One approach to this is to maintain a small clearance between the piston and cylinder. This solution was proposed for a microscale actuator design where the piston is enclosed in a compartment filled with fluid. However, leakages occur at the location where the moving parts go out of this compartment (*8*), thus preventing its use for medical applications. Moreover, such mechanism requires two pressure connections on both sides of the piston, which can complicate the system design or require the use of a fluid resonator (*9*). For practical deployment, it is desirable to find an approach with a seal between the outer cylinder and the piston of the pneumatic mechanism. In certain cases, this can be achieved by using inflatable and deformable parts (*10*–*12*), but their design with micrometric precision at the tip of a capillary remains highly challenging. Therefore, we choose to use surface tension forces between air and gas to provide the seal. Surface tension effects scale linearly with size and are therefore desirable when considering micrometer-sized features. Unlike friction forces, they provide smooth and well-modeled forces and have been used for the control (*13*) and propelling (*14*) of floating microrobots. Moreover, capillary force actuation also provides compliance, which is useful against shocks and for interaction with soft substrates. This liquid seal approach was used previously at the millimeter scale for actuators fabricated by subtractive manufacturing (*15*) and was also integrated into two-dimensional (2D) substrates (*16*, *17*). In this work, we propose a compact micropiston designed at the tip of a 140-μm flexible capillary to allow the use of such actuators for microcatheter-based interventions.

For a micrometer-scale pneumatic actuator using liquid to close the gap between the piston and cylinder, a high-pressure difference is necessary to deform the liquid/gas interface. Below this threshold pressure difference, the liquid acts as a seal for the piston, as shown in Fig. 1A. Similar phenomena have been used for removing bubbles

[1]Hamlyn Centre, Imperial College London, London, UK. [2]Institute of Medical Robotics, Shanghai Jiao Tong University, Shanghai, China.
*Corresponding author. Email: a.barbot@imperial.ac.uk (A.B.); gzyang@sjtu.edu.cn (G.-Z.Y.)

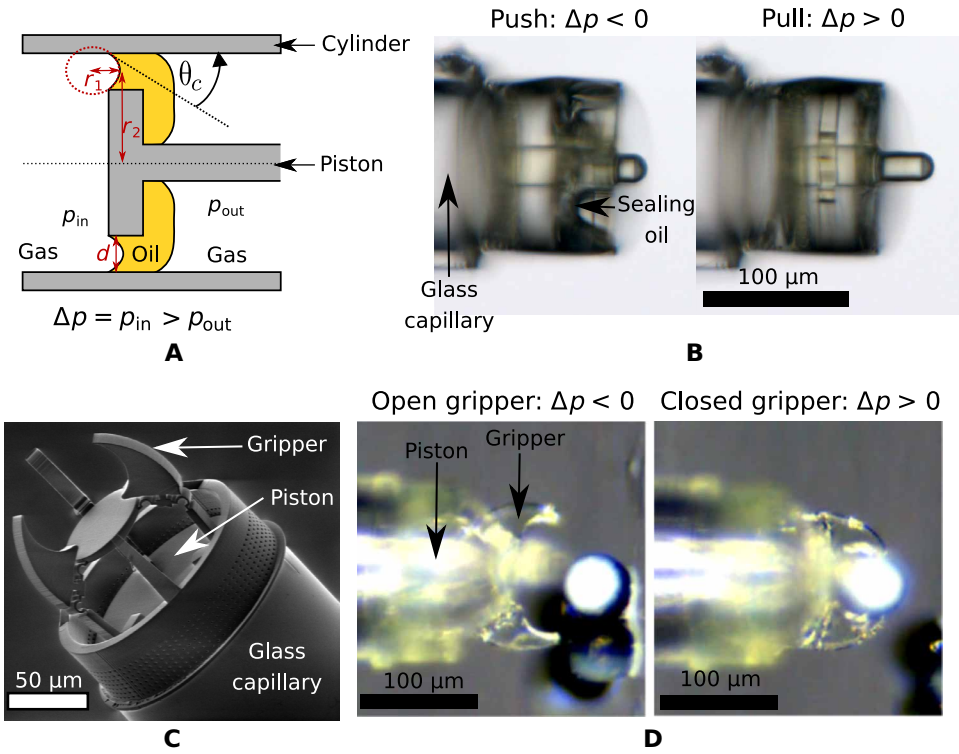

Fig. 1. Principle of operation of the proposed micropiston. (**A**) Schematic of the microscale physical interaction at the seal formed by surface tension between gas and liquid. (**B**) Microscopic pictures of the micropiston actuation. The corresponding actuation video is available in movie S1. (**C**) The SEM picture of a micropiston integrated into a compliant gripper. (**D**) Demonstration of the gripper while grasping a microsphere.

in microfluidic chips (*18*), passive pressure difference valves (*19*), and microactuators using electrowetting (*20*). In this article, we propose a monolithic fabrication approach based on two-photon polymerization (2PP) to create a microscale tool capable of fitting within a 150-µm cube space and controlled by a pneumatic actuator that relies on a liquid seal made with silicone oil (SYLGARD 184 Silicone Elastomer). To ensure biocompatibility of the microactuators, both the photoresist (*21*) and the silicone oil (*22*) used to fabricate the device are noncytotoxic materials. Figure 1B gives an overview of the piston actuation. We first propose a model of the liquid seal to derive the relationship between the maximal pressure difference to the surface energy between the liquid and the 2PP photoresist. This model was then used to design and fabricate an appropriate geometry, which was used for experimental measurements to compare with theoretical predictions of pressure required to break the oil seal. We then characterized the piston's mechanical behavior by measuring the relationship between displacement and force due to varying applied pressure amplitudes and frequencies. The durability of the devices was then assessed by repeatedly testing under cyclic pressure loading and unloading. Last, we show how this micropiston fabrication method can be integrated into a more complex microsystem by actuating a compliant microgripper at the capillary tip, as shown in the SEM image in Fig. 1C. As a case study, we demonstrate its functionality by grasping, transporting, and releasing a 50-µm microsphere, as shown in Fig. 1C. Preliminary work on the fabrication of air micropiston actuated air underwater has been presented at the International Conference on Manipulation, Automation and Robotics at Small Scales (MARSS) 2018 as an oral presentation.

RESULT

Surface tension seal model

At a liquid/gas interface, there is a difference between the strong cohesion force of the liquid molecules with other liquid molecules and the weak forces between the liquid molecules and gas molecules. This induces a pressure difference between the two phases. The Laplace equation describes this pressure difference as a function of the curvature of the interface

$$\Delta p = \sigma\left(\frac{1}{r_1} + \frac{1}{r_2}\right) \quad (1)$$

with σ representing the surface tension between the liquid and the gas, and r_1 and r_2 denoting the two principal minimal radii of curvature of the gas/water interface.

We are interested in the case where a liquid volume forms a seal in a micropiston gap. In this configuration, the liquid seal remains intact as long as the pressure difference (Δp) on the two sides of the piston does not exceed the threshold to push the gas through the cylinder piston gap. The wetting state of the piston and cylinder surface imposes the following two scenarios.

In the first scenario, when the liquid is pushed away, the surface is dry. This is illustrated in Fig. 2 (inset A). In this case, the angle formed between the air/liquid interface and the solid (θ_c) needs to be smaller than the advancing contact angle. By using the notation used in Fig. 1A, we obtain

$$r_1 > \frac{d}{2\cos\theta_c} \quad (2)$$

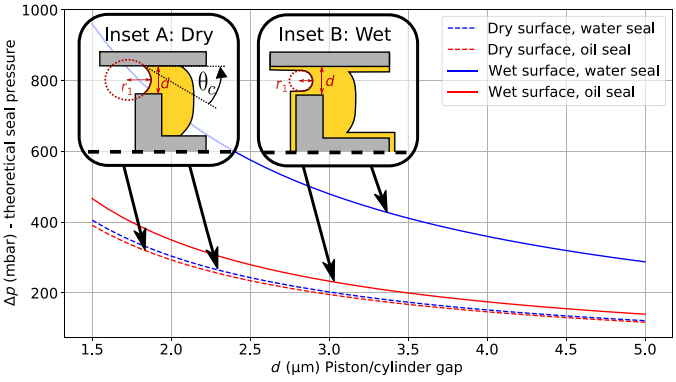

Fig. 2. Theoretical evolution of seal maximum pressure difference value with the piston cylinder gap. Scenario with wet and dry surface is shown for water and the chosen silicone oil.

where d is the gap between the piston and the cylinder. Because, in this work, r_2 is more than 10 times larger than r_1, we can neglect its impact on Eq. 1. Therefore, the seal is intact when the following condition is held

$$\Delta p_{\mathrm{dry}} < \frac{2\sigma\cos\theta_c}{d} \tag{3}$$

In the second scenario when the liquid is pushed away, the surface remains wet. This is illustrated in Fig. 2 (inset B). In this case, by assuming an infinitesimally small wetting layer, the minimal radius of curvature (r_1) to push the air through the seal gap is

$$r_1 > \frac{d}{2} \tag{4}$$

and, therefore, the maximum pressure difference (Δp_{wet}) conditions is

$$\Delta p_{\mathrm{wet}} < \frac{2\sigma}{d} \tag{5}$$

Figure 2 describes the theoretical relationship between the piston/cylinder gap versus the maximal pressure difference supported by the liquid seal for the two different conditions (as described above and illustrated in the figure insets). For this calculation, the surface energy of water and silicone oil was considered to be 0.072 N m^{-1} (*23*) and 0.035 N m^{-1} (*24*), respectively. The viscosity of the silicone oil was 5.1 Pa·s. The contact angle with the piston material (IP-dip) was measured to be 65° ± 3.9° for water and 33° ± 3° for silicone oil.

There are two primary trends that can be observed from these curves. First, the wet condition always results in a larger pressure difference because the surface curvature radius needs to be smaller to fit through the gap. Second, the calculation for oil and water remains identical to the dry condition. Water has a greater surface energy than silicone oil, but this can be compensated for in Eq. 3 by water's large contact angle with the photoresist.

In the following sections, most of the characterization of the piston was performed with silicone oil. However, we also measured the breaking threshold of the seal in water for comparison. From this, we can deduce whether the piston is in the dry or wet condition and estimate the piston/cylinder gap size during the actuation. It is challenging to estimate this gap during actuation owing to fabrication variability, resulting in the likely imperfect concentricity of the piston and outer cylinder.

Fabrication and experimental setup

A 2PP direct laser writing system (Photonic Professional GT, Nanoscribe) was used to directly fabricate the micropiston and microgripper onto the end of the glass capillaries. Figure 3 (A and B) shows side by side the schematic and scanning electron microscope picture of the micropiston, respectively.

To prevent the central part of the micropiston structure from moving during 2PP fabrication, a low-stiffness spring was printed to link it to the base of the outer cylinder. This spring is shown in Fig. 3A. After fabrication, the capillary micropiston assembly was dipped in a 20% silicone oil/80% isopropyl alcohol solution. By capillary action, the solution travels inside the capillary through the piston/cylinder gap. The mechanism was then left to dry for at least 2 min, allowing the alcohol to evaporate and leaving behind oil in the most confined space located at the piston/cylinder gap. This step was repeated four to six times until the seal of oil on the piston could be observed under a microscope by a layer more than 10 μm on one of the sides. Movie S2 shows a recording of this step.

After the fabrication of the oil seal, the assembly was connected to a pneumatic circuit. This circuit consisted of two pressure reservoirs connected to a pump and a vacuum generator (Dolomite, Mitos Fluika pump), respectively, to apply a positive or negative pressure difference to the piston. A switch allowed the connection of the capillary between these two reservoirs to be swapped as shown in Fig. 3B. In this experiment, the switch had a maximum operating frequency of 15 Hz. Figure 3C shows a schematic of this pressure circuit. The micropiston could then be characterized by either measuring its displacement or the force generated. For the displacement, a microscope camera (AxioZoom V16, Zeiss) (2 μm pixel^{-1} resolution) recorded the movement of the piston. This recording was then analyzed frame by frame by custom software, using OpenCV (*25*) for image processing, which tracked the piston position relative to the cylinder. To measure the piston force, a capacitive force sensor was used (FEMTO tool FT-S100000 Microforce Sensing Probe). Both the piston and the sensor were each mounted on the top of a 4–degree of freedom micromanipulator robot (Imina miBot Micro/Nanomanipulators). The tip of the force sensor was placed close to the retracted piston, as can be seen on the right of Fig. 3, with a maximum distance of 5 μm.

Micropiston characterization

By operating the switch between the pressurized reservoir at regular intervals, a square wave pressure input was applied on the inner side of the piston with a 50% duty cycle. In the following section, we quantify this signal by considering the difference between the applied pressure and ambient pressure, which correspond to Δp in the previous equations. Therefore, we first characterized the displacement amplitude of the piston for an applied square wave pressure difference. The position of the piston was analyzed by tracking the piston tip and the cylinder edge on recorded microscope view. More details on the tracking are available in Materials and Methods and section S2.

Figure 4A shows this result for a frequency up to 8 Hz and an input pressure difference with amplitudes ranging from 100 mbar (50 to −50 mbar) to 400 mbar (200 to −200 mbar). For frequency lower than 2 Hz and pressure difference higher than 100 mbar, the maximum achievable displacement was 35 μm. For higher frequencies, this displacement was reduced. This damping is mainly due to viscous drag of the oil seal moving in between the piston and the cylinder. The characterization of the force amplitude for a square wave input

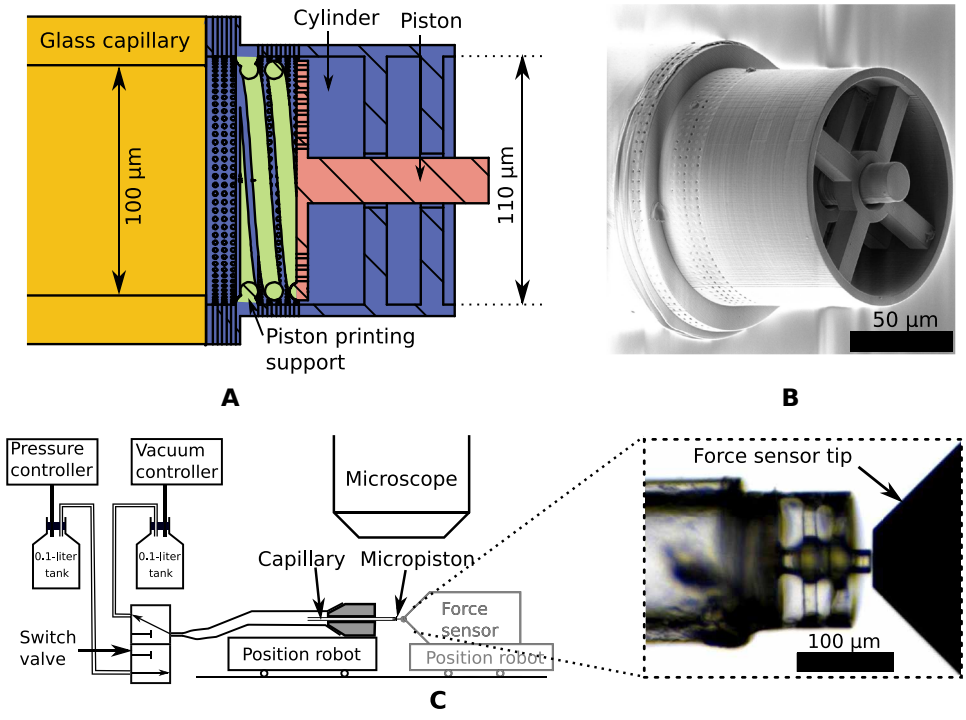

Fig. 3. Micropiston fabrication and setup. (**A**) Cross-sectional view of the micropiston design. (**B**) SEM image of the piston printed by 2PP directly on the tip of a glass capillary. (**C**) Pneumatic circuit and imaging setup for the proposed micropiston actuation. The figure displays the two possible configurations: one to study the displacement of the piston and the other to study the corresponding force.

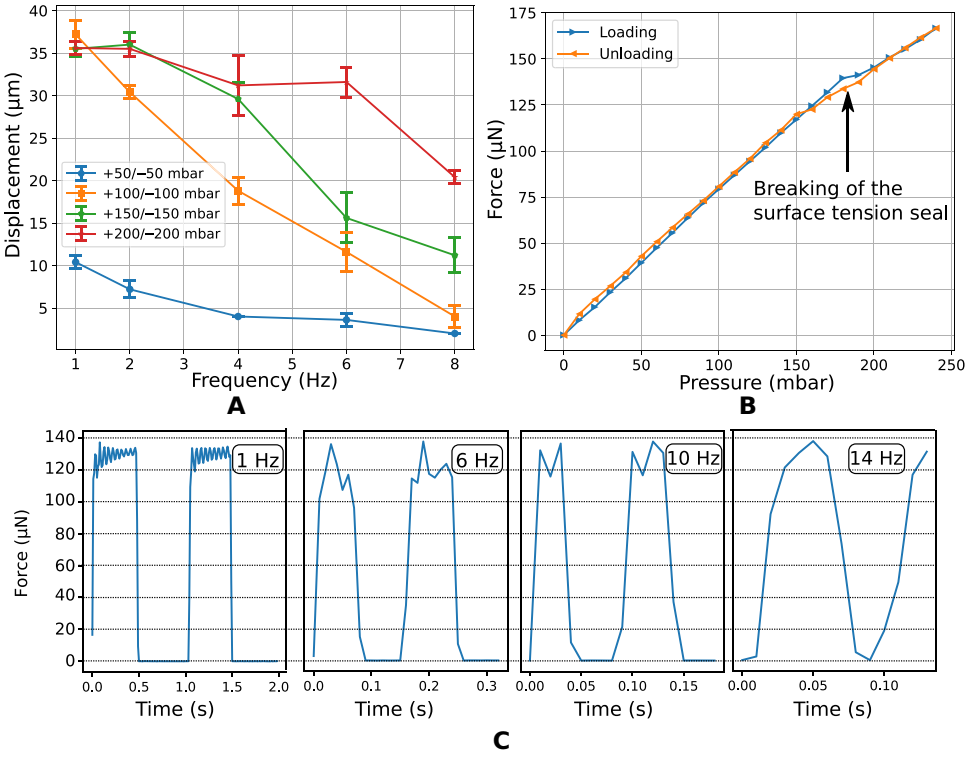

Fig. 4. Displacement and force characterization of the micropiston for different pressure inputs and frequencies. (**A**) Amplitude of the micropiston at different frequencies and with different supplied pressure differences. Each data point is derived from the average amplitude of five full cycles of actuation, and the associated error bar of each data point shows the SD. (**B**) Graph of the force measured at the piston tip during a loading/unloading pressure cycle. (**C**) Graph of the force measured at the piston tip actuated by an input pressure with a square waveform at various frequencies (1, 6, 10, and 14 Hz). Intermediate frequency is available in section S1.

pressure at different frequencies did not show substantial damping, as can be seen in Fig. 4. Therefore, we can conclude that pressure is not lost in the pneumatic circuit with increasing frequency. In the force experiment, the movement of the piston was reduced to a maximum of 5 μm for the piston to contact the force sensing probe and thus the viscous drag from the seal movement was reduced. Moreover, the maximum force does not seem to reduce between cycles.

The relationship between the input pressure applied to the piston and the consequent force applied by the piston to the tip of the sensor was measured. The input pressure ranged from 0 to 240 mbar in 10-mbar steps, as presented in Fig. 4B. For applied pressures up to 160 mbar, this relationship was linear with a slope of 0.79 mbar μN^{-1}. This slope is less than, but still on the same order of magnitude as, the theoretical slope based on the assumption that the pressure is applied on all of the cylinder surfaces, in which case the value would be 0.95 mbar μN^{-1}. At 180 mbar, the oil seal breaks and thus reduces the pressure difference between the two sides of the piston. This is reflected in the graph describing the input pressure–to–output force relationship in Fig. 4B. With the seal broken, the slope reduces to 0.54 mbar μN^{-1}.

While cycling the pressure, a hysteresis between these two regimes was observed as the seal broke between 180 and 190 mbar and was fully recovered when the pressure was reduced back to under 150 mbar. A video recording of the breaking of the seal in oil and water is shown in movie S4, along with microscope images in section S3. The breaking of the seal was measured on five consecutive experiments with both oil and water seal. For oil, breaks happened in between 185 and 208 mbar. For experiment in water, the piston was immersed in a water container to create the seal and breaks happened in between 357 and 402 mbar.

As water evaporates quickly in air, it is therefore impossible to form a droplet water seal that can be stable over prolonged periods of time. To measure the maximum pressure difference of the seal, in the case of water, the piston was immersed in a container of water. Therefore, all of the external volume of the piston and the piston/cylinder gap were filled with water by capillarity. In this experiment, only one gas/liquid interface was created, allowing an efficient seal only while pushing with a positive pressure on the inner part of the piston. A gas/liquid interface can sustain a difference of pressure owing to the energy change required to expand the liquid front. It is the base mechanism of most passive microfluidic valves (*19*). However, in the case of the piston/cylinder gap, this pressure difference is smaller than the one required to bend the liquid surface through the micrometer-scale gap. The pressure difference required to expand the liquid interface through the piston/cylinder gap was only 5 mbar, as reported in section S4.

Multiple loading and unloading tests with a 160-mbar pressure difference were also conducted, with an oil seal piston, to study the repeatability of the actuation and reproducibility of the force measurements. The same pressure control setup was used for each of these tests, and the force at the piston tip was measured by the force sensor. Figure 5 shows a superposition of the measured forces for 80 consecutive tests, as well as the maximum difference and SD between the tests.

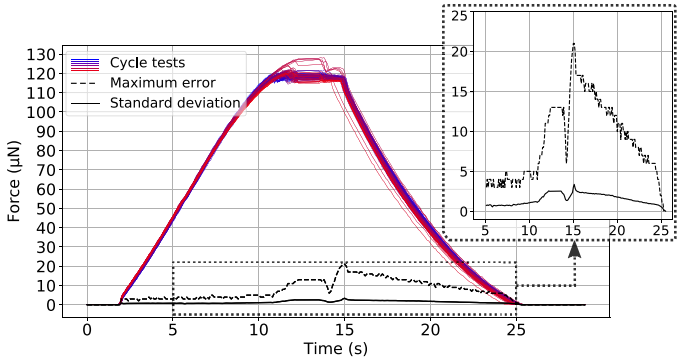

Fig. 5. Superposition of 80 piston force curves for the same input pressure difference signal. Each color, plotted in a gradient from blue to red, represents one test. The maximum error and SD of the curves show good repeatability of the force exerted on the sensor by the piston.

Microgripper

The proposed micropiston offers displacement and force control in a compact system at the microscale by using a 2PP monolithic fabrication approach. This allows the piston design to be integrated at the tip of a flexible capillary, hence opening the path to the design of various piston-based micromechanical tools at the end of the microcatheter. To demonstrate this, and to assess the practical value of such microscale actuator, a pneumatic gripper was designed by linking the piston and the cylinder to a compliant mechanism.

The compliant structure transforms the axial displacement of the piston into the closing of a three-finger gripper, as shown in the cross-sectional view of the design in Fig. 6A. The design and fabrication of a similar mechanism printed by 2PP have previously been discussed (*7*).

With this gripper, we successfully performed a task involving the grasping, transport, and release of a 50-μm microsphere as illustrated in Fig. 6 (B to D). For this experiment, the gripper was fixed to a three-axis micromanipulator (Thorlab PT3) and held horizontally. The 50-μm bicolored polyethylene microspheres (Cospheric HCMS-BLK-WHT) were placed on a microscope glass slide. The pattern on the microsphere allows for better visualization and contrast during the experiments. The microscope glass slide was fixed 20° from the vertical to ensure adequate microscope visualization during the experiment.

DISCUSSION

Here, we have demonstrated the practical usage of a pneumatically actuated micropiston using a liquid seal technique. The linear behavior between the measured force and the pressure input as shown in Fig. 4B demonstrates a clear advantage of the pneumatic force solution for microactuators for which a relatively large displacement is required. This linearity facilitates the prediction of applied force, hence opening the way for simple and precise automated open-loop actuation. Moreover, Fig. 5 shows that the force controlled by the pressure input is repeatable over time with a maximum SD less than 3%. These repeatability experiments show that only less than 15% of the tests present a bigger error (up to a maximum of 20%) whereas the rest of them have the same trend as each other. The error of the outlier tests may be attributed to the automation of the pressure command as they display a bigger force than the average tests. One advantage of this micropiston is that it is a compact microactuator that can produce both large displacement and force. It has a force-to-volume ratio of around 50 mN mm^{-1} while being capable of achieving a displacement of 40 μm. This force-to-volume ratio is

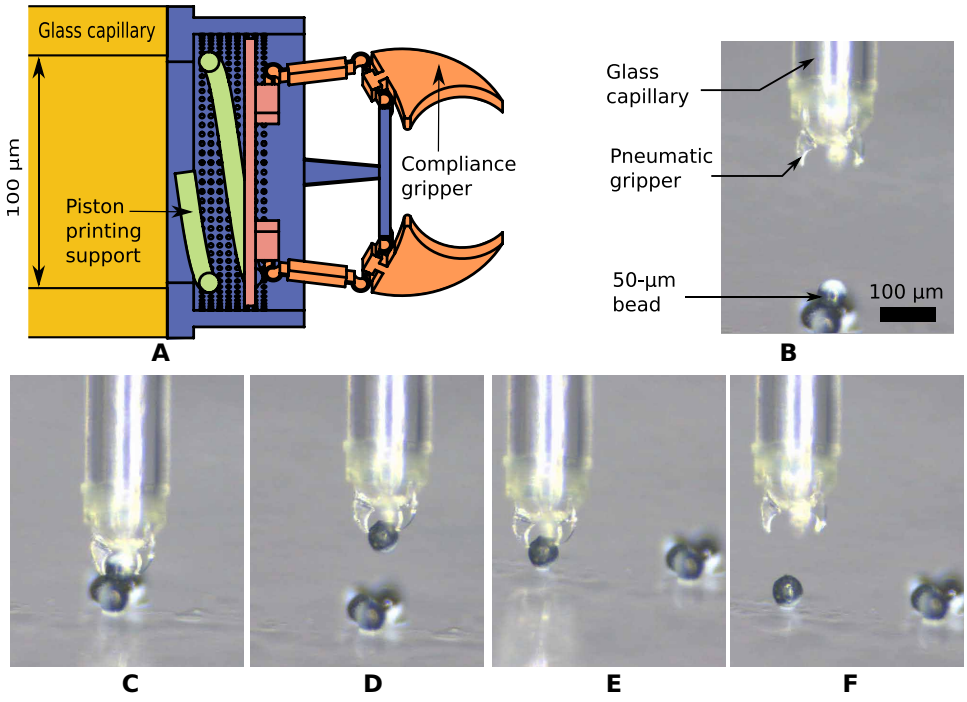

Fig. 6. Micropiston-based compliant gripper. (**A**) The design of the compliant gripper on top of the micropiston. (**B**) A microscope view of 50-µm microsphere manipulation with the pneumatic gripper, demonstrating (**C**) grasp, (**D** and **E**) transport, and (**F**) release of the microsphere. A video record of the experiment is available in movie S3.

comparable to the maximum force of microelectromechanical systems (MEMS) comb drive actuators with a maximum displacement limited by a finger spacing of 2 µm (*26*). Higher displacement is possible, but the finger spacing is inversely proportional to the force (*27*). The measurement of the piston force with a step increase of the pressure presented in Fig. 4B shows a 17% difference between measured force and the theoretically calculated force (which assumed that the input pressure is fully experienced by the piston plate). Part of the sealing oil remaining on the high-pressure surface of the piston is the main factor behind this difference. If this air/oil interface stuck on the piston bends while the pressure increases, a drop in pressure [as explained by the Laplace equation (Eq. 1)] will reduce the total force on the piston. Moreover, the contact with the low-stiffness spring used to fix the piston plate during the printing process also created two small asperities. These asperities may be filled with oil by capillarity, thus increasing the pressure drop areas in the inner plate of the piston. The difference between the measurement of the seal breaking between water and the silicone oil presented suggests that the micropiston material is wet in all the cases studied. The measured seal breaking pressure difference is two times greater for water than oil, which is the ratio between these two surface tensions. The wet model implies that the minimal breaking pressure difference depends only on the surface energy in a linear fashion, as shown in Eq. 6. Local changes in the wetting condition of the material around the seal may explain the maximum 12% variation for the different measurements.

By assuming the wet scenario and using Fig. 2, we can deduce that the maximum piston/cylinder gap is between 3.5 and 4 µm. As the designed gap was 2 µm, this seems to suggest that the piston is slightly askew with respect to the outer cylinder. It is likely that one side of the piston is almost touching the cylinder and, thus, leaving an approximately 4-µm gap on the opposite side. This is confirmed by the observation of the liquid seal breaking at a specific location (as seen in section S3), which probably pushes the piston to one side.

There is no self-alignment of the piston due to the meniscus at least for the steady state. The two contributing capillary forces, which are the surface tension of the triple line and the pressure difference, are both zero on the lateral axis. The surface tension is zero because, as demonstrated, the system is fully wet and therefore there is no triple line connected to the piston. The pressure is zero because the ring around the piston forms a single drop with uniform pressure that applies the same force on its surface for the alignment or misalignment case. However, when the piston is moving, the meniscus acts as a lubrication layer and thus provides a higher lift force on the side of the piston that is closer to the cylinder wall (*28*), which results in its alignment.

An important design consideration is the choice of the sealing material. In this study, we chose silicone oil because it does not evaporate in our experimental conditions, thus allowing a stable seal during experiments and even over several months for the same micropiston. Another motivation behind choosing silicone was that this material can be used safely in vivo and it is routinely used in surgery (*22*). It should be noted that the usage of this type of silicone oil comes with certain drawbacks in performance. It has a low surface energy and a 2-µm seal that can break starting from 185 mbar, whereas solution with water can withstand pressures up to 360 mbar. Liquid metal (*15*) could withstand even higher pressures. Moreover, the high viscosity of the oil induces a large damping of the displacement due to viscous friction forces. However, the combination of low surface energy and high viscosity allows both an easy recovery from the breaking of the seal, as well as a limitation of the airflow rate while the seal is broken. This can be of a particular interest to propose a robust design that can "self-heal" in the event of the maximum

pressure threshold being exceeded. Even after the oil seal is broken, the piston can still operate at lower actuation frequencies with a slightly lower pressure-to-force relationship, as demonstrated in Fig. 4B.

In summary, we have presented the design, fabrication, and characterization of a micropiston printed at the tip of a 140-μm capillary capable of 35-μm displacement with a maximum output force of 135 μN with a driving pressure of 185 mbar. A key aspect of the proposed design was the use of a liquid seal allowing such a large pressure difference without a leak between the two sides of the piston. The method presented is a viable alternative to solid joints, which exhibit dominant friction force over the actuation force at this scale.

Here, we explained why the silicone oil is a good candidate for such sealing as it is biocompatible and can recover easily from a break of the sealing in the event of an excessive pressure difference. However, applications where high-frequency (>10 Hz) displacement is required should use a liquid with lower viscosity. Extension of this work would be to assess the cutoff of the piston displacement by proposing a model of the liquid seal depending on the geometry and liquid viscosity and surface tension. The first question will be to assess whether a spring/damper/mass system is sufficient to model the seal compartment as for a liquid bridge (*29*) and under which consideration.

Biocompatibility and patient safety of the mechanism will need to be validated for different in vivo applications. When used for endovascular applications, traces of silicone oil could be problematic in the bloodstream, and the potential for embolisms would need to be investigated as well as the use of alternative biodegradable oils. However, for natural orifice surgeries, where the oil will be washed away by natural secretion, the use of silicone oil should not pose a major problem. For tissue insertion, a small quantity of silicone may remain inside the tissue. This has already been proven to be safe for the eye (*22*) but would need to be investigated for other organs. Air leakage is another concern for endovascular applications and particularly inside the arterial system. This should be prevented by avoiding pressures close to the seal's breaking threshold. In organ tissues, a small air quantity will slowly dissolve in the bloodstream and bubbles in the venous system will be filtered by the lung (*30*). This quantity needs to remain small [the lethal air dose in the venous system is around 200 ml for an adult (*31*)], and a leak detection system should be implemented in any case to stop the airflow. Overall, we have demonstrated that such micropiston could provide the actuation mechanism to drive a microtool at the tip of a catheter. We realized a compliant gripper and demonstrated the grasping, transport, and release of a 50-μm microsphere. Such pneumatic mechanisms could find many applications for microcatheters in surgery. Their relatively high force compared to their size makes them a good candidate for microbiopsy tools or active micro-optics mechanism. It would be beneficial to examine the fabrication of selective hydrophobic regions to control the wetting condition. This would allow more control over the droplet position and its topology, so that they can be used as compliant fluid joints in more complex and self-aligned mechanisms.

MATERIALS AND METHODS

Piston printing

A 2PP direct laser writing system (Photonic Professional GT, Nanoscribe) was used to fabricate the micropiston and gripper onto the end of the glass capillary. The outer diameter of the capillary (TSP100170, Polymicro Technologies) without cladding was 140 μm, and the inner diameter was 100 μm. IP-Dip photoresist was used following the same protocol as described in previous work (*7*). The main modification to the printing technique was the temporary use of ultraviolet-curable glue to plug the proximal end of the capillary to prevent the photoresist from traveling too far up the hollow channel, thus impeding the removal of the viscous photoresist during the first step of the development in PGMEA for 45 min. To ensure a proper development of the part between the capillary tip and the piston, 2-μm holes were included in the design. These holes were then blocked by the silicone oil and could theoretically withstand a pressure difference two times larger than the pressure difference withstood by the liquid seal between the piston and the cylinder as explained in Eq. 1. The proximal end of the capillary was then cut and the PGMEA was pumped in through the capillary for 20 min. Isopropyl alcohol was then pumped through the capillary for 5 min to rinse the structure.

Contact angle measurement

To measure the contact angle between the water or silicone oil and polymerized IP-Dip, we first printed, by 2PP, a circle of photoresist with a radius of 3 mm and a thickness of 1 μm. The contact angle with a 5-μl droplet of deionized water and the silicone oil was measured on a Keyence digital microscope VHX 2000 calculated using spherical approximation (ImageJ, plugin Contact Angle).

Piston displacement tracking

The tracking of the piston tip of the video was performed by using the OpenCV library. To automatically determine the displacement of the moving piston with respect to the outer cylinder, a custom OpenCV-based program was written. This program analyzes videos of the cycling piston frame by frame to track its movement over time. A uniform white background behind the printed structure facilitates identification of the edges of the structure using a grayscale threshold. The user defines a grayscale threshold value and selects on the image two horizontal lines (denoted by red and green solid lines in section S2) along which to search for the edge of the piston and cylinder. The program searches for the rightmost point at which the user-defined pixel threshold is exceeded, and the identified edge is marked with a black circle. The horizontal difference between these two detected edges corresponds to the piston displacement for a given frame. Figure S2 (A and B) shows the piston at the two extreme positions of its stroke. The tracking program's source code, with a video example, is available at https://github.com/micropoz/line_tracking.

SUPPLEMENTARY MATERIALS

Supplementary material for this article is available at http://advances.sciencemag.org/cgi/content/full/6/22/eaba5660/DC1

REFERENCES AND NOTES

1. G.-Z. Yang, J. Bellingham, P. E. Dupont, P. Fischer, L. Floridi, R. Full, N. Jacobstein, V. Kumar, M. McNutt, R. Merrifield, B. J. Nelson, B. Scassellati, M. Taddeo, R. Taylor, M. Veloso, Z. L. Wang, R. Wood, The grand challenges of *Science Robotics*. *Sci. Robot.* **3**, eaar7650 (2018).
2. O. M. Wani, H. Zeng, A. Priimagi, A light-driven artificial flytrap. *Nat. Commun.* **8**, 1 (2017).
3. F. Ullrich, K. S. Dheman, S. Schuerle, B. J. Nelson, in *Magnetically Actuated and Guided Milli-gripper for Medical Applications* (IEEE, 2015), pp. 1751–1756.
4. M. N. Faddis, W. Blume, J. Finney, A. Hall, J. Rauch, J. Sell, K. T. Bae, M. Talcott, B. Lindsay, Novel, magnetically guided catheter for endocardial mapping and radiofrequency catheter ablation. *Circulation* **106**, 2980–2985 (2002).

5. V. Lalande, F. P. Gosselin, S. Martel, Catheter steering using a magnetic resonance imaging system. *Conf. Proc. IEEE Eng. Med. Biol. Soc.* **2010**, 1874 (2010).
6. M. De Volder, D. Reynaerts, Pneumatic and hydraulic microactuators: A review. *J. Micromech. Microeng.* **20**, 043001 (2010).
7. M. Power, A. J. Thompson, S. Anastasova, G.-Z. Yang, A monolithic force-sensitive 3D microgripper fabricated on the tip of an optical fiber using 2-photon polymerization. *Small* **14**, e1703964 (2018).
8. M. De Volder, F. Ceyssens, D. Reynaerts, R. Puers, Microsized piston-cylinder pneumatic and hydraulic actuators fabricated by lithography. *J. Microelectromech. Syst.* **18**, 1100–1104 (2009).
9. U. Gebhard, H. Hein, E. Just, P. Ruther, in *Proceedings of International Solid State Sensors and Actuators Conference (Transducers' 97)* (IEEE, 1997), vol. 2, pp. 761–764.
10. X. Yang, Y.-C. Tai, C.-M. Ho, in *Proceedings of International Solid State Sensors and Actuators Conference (Transducers' 97)* (IEEE, 1997), vol. 1, pp. 45–48.
11. K. Moussi, J. Kosel, 3-D printed biocompatible micro-bellows membranes. *J. Microelectromech. Syst.* **27**, 472–478 (2018).
12. J. Paek, I. Cho, J. Kim, Microrobotic tentacles with spiral bending capability based on shape-engineered elastomeric microtubes. *Sci. Rep.* **5**, 10768 (2015).
13. A. Barbot, H. Tan, M. Power, F. Seichepine, G.-Z. Yang, Floating magnetic microrobots for fiber functionalization. *Sci. Robot.* **4**, eaax8336 (2019).
14. R. Terrazas, A. de Maeijer, A. Bolopion, M. Gauthier, M. Kinnaert, P. Lambert, Thermocapillary micromanipulation: Force characterization and Cheerios interactions. *J. Micro-Bio Robot.* **15**, 13–22 (2019).
15. M. De Volder, J. Peirs, D. Reynaerts, J. Coosemans, R. Puers, O. Smal, B. Raucent, A novel hydraulic microactuator sealed by surface tension. *Sensor. Actuat. A. Phys.* **123**, 547 (2005).
16. A. P. Papavasiliou, A. P. Pisano, D. Liepmann, in *Transducers 01 Eurosensors XV* (Springer, 2001), pp. 912–915.
17. J. J. Sniegowski, E. J. Garcia, in *Micro-Optics/Micromechanics and Laser Scanning and Shaping* (International Society for Optics and Photonics, 1995), vol. 2383, pp. 46–64.
18. C. Liu, J. A. Thompson, H. H. Bau, A membrane-based, high-efficiency, microfluidic debubbler. *Lab Chip* **11**, 1688–1693 (2011).
19. P. Man, C. Mastrangelo, M. Burns, D. Burke, in *Proceedings MEMS 98. IEEE. Eleventh Annual International Workshop on Micro Electro Mechanical Systems. An Investigation of Micro Structures, Sensors, Actuators, Machines and Systems (Cat. No. 98CH36176)* (IEEE, 1998), pp. 45–50.
20. J. Kedzierski, E. Holihan, R. Cabrera, I. Weaver, Re-engineering artificial muscle with microhydraulics. *Microsyst. Nanoengineering* **3**, 17016 (2017).
21. F. Klein, B. Richter, T. Striebel, C. M. Franz, G. von Freymann, M. Wegener, M. Bastmeyer, Two-component polymer scaffolds for controlled three-dimensional cell culture. *Adv. Mater.* **23**, 1341–1345 (2011).
22. V. Pagot-Mathis, X. Benouaich, A. Mathis, I. Rico-Lattes, A. Dumoulin, Management of complicated retinal detachment using a heavy silicon oil as temporary tamponade. *J. Fr. Ophtalmol.* **29**, 137–145 (2006).
23. N. R. Pallas, Y. Harrison, An automated drop shape apparatus and the surface tension of pure water. *Colloids Surf.* **43**, 169–194 (1990).
24. F. Barca, T. Caporossi, S. Rizzo, Silicone oil: Different physical proprieties and clinical applications. *Biomed. Res. Int.* **2014**, 502143 (2014).
25. G. Bradski, The OpenCV Library, *Dr. Dobb's Journal of Software Tools* (2000).
26. M. J. Sinclair, ITHERM 2000, in *The Seventh Intersociety Conference on Thermal and Thermomechanical Phenomena in Electronic Systems* (Cat. No. 00CH37069) (IEEE, 2000), vol. 1, pp. 127–132.
27. M. González, P. Zheng, E. Garcell, Y. Lee, H. B. Chan, Comb-drive micro-electro-mechanical systems oscillators for low temperature experiments. *Rev. Sci. Instrum.* **84**, 025003 (2013).
28. B. J. Hamrock, *Fundamentals of Fluid Film Lubrication* (NASA, 1991).
29. J.-B. Valsamis, M. Mastrangeli, P. Lambert, Vertical excitation of axisymmetric liquid bridges. *Eur. J. Mech. B Fluids* **38**, 47–57 (2013).
30. D. Z. H. Levett, I. L. Millar, Bubble trouble: A review of diving physiology and disease. *Postgrad. Med. J.* **84**, 571–578 (2008).
31. T. J. K. Toung, M. I. Rossberg, G. M. Hutchins, Volume of air in a lethal venous air embolism. *Anesthesiology.* **94**, 360–361 (2001).

Acknowledgments: We thank M. Abdelaziz for helpful discussions and J. A. Kim for assisting with 2PP fabrication. **Funding:** This work was supported by EPSRC—EP/P012779/1—Micro-Robotics for Surgery. This work is part of the Fiberbot project. **Author contributions:** A.B. proposed and designed the piston and liquid sealing setup, performed the characterization and modeling, and assisted in the fabrication process. M.P. designed and realized the microgripper and performed the 3D printing at the fiber tip. F.S. designed and performed the contact angle measurement and supported A.B. in data acquisition and analysis. G.-Z.Y. proposed and designed the fiberbot concept, initiated the project (microrobotics for surgery), secured funding, and supervised all steps of the project. **Competing interests:** The authors declare that they have no competing interests. **Data and materials availability:** All data needed to evaluate the conclusions in the paper are present in the paper and/or the Supplementary Materials. Additional data related to this paper may be requested from the authors.

Submitted 13 December 2019
Accepted 1 April 2020
Published 27 May 2020
10.1126/sciadv.aba5660

Citation: A. Barbot, M. Power, F. Seichepine, G.-Z. Yang, Liquid seal for compact micropiston actuation at the capillary tip. *Sci. Adv.* **6**, eaba5660 (2020).